Acta Biomaterialia 128 (2021) 130–142

Contents lists available at ScienceDirect

Acta Biomaterialia

journal homepage: www.elsevier.com/locate/actbio

Full length article

Affinity-bound growth factor within sulfated interpenetrating network bioinks for bioprinting cartilaginous tissues

Bin Wang[a,b], Pedro J. Diáz-Payno[a,b], David C. Browe[a,b,c], Fiona E. Freeman[a,b], Jessica Nulty[a,b], Ross Burdis[a,b], Daniel J. Kelly[a,b,c,d,*]

[a] Trinity Centre for Biomedical Engineering, Trinity Biomedical Sciences Institute, Trinity College Dublin, Dublin, Ireland
[b] Department of Mechanical, Manufacturing & Biomedical Engineering, School of Engineering, Trinity College Dublin, Dublin, Ireland
[c] Advanced Materials and Bioengineering Research Centre (AMBER), Royal College of Surgeons in Ireland and Trinity College Dublin, Dublin, Ireland
[d] Department of Anatomy, Royal College of Surgeons in Ireland, Dublin, Ireland

ARTICLE INFO

Article history:
Received 12 December 2020
Revised 7 April 2021
Accepted 8 April 2021
Available online 15 April 2021

Keywords:
3D bioprinting
Sulfated IPN
Growth factor
Control release
Articular cartilage
Tissue engineering

ABSTRACT

3D bioprinting has emerged as a promising technology in the field of tissue engineering and regenerative medicine due to its ability to create anatomically complex tissue substitutes. However, it still remains challenging to develop bioactive bioinks that provide appropriate and permissive environments to instruct and guide the regenerative process *in vitro* and *in vivo*. In this study alginate sulfate, a sulfated glycosaminoglycan (sGAG) mimic, was used to functionalize an alginate-gelatin methacryloyl (GelMA) interpenetrating network (IPN) bioink to enable the bioprinting of cartilaginous tissues. The inclusion of alginate sulfate had a limited influence on the viscosity, shear-thinning and thixotropic properties of the IPN bioink, enabling high-fidelity bioprinting and supporting mesenchymal stem cell (MSC) viability post-printing. The stiffness of printed IPN constructs greatly exceeded that achieved by printing alginate or GelMA alone, while maintaining resilience and toughness. Furthermore, given the high affinity of alginate sulfate to heparin-binding growth factors, the sulfated IPN bioink supported the sustained release of transforming growth factor-β3 (TGF-β3), providing an environment that supported robust chondrogenesis *in vitro,* with little evidence of hypertrophy or mineralization over extended culture periods. Such bioprinted constructs also supported chondrogenesis *in vivo*, with the controlled release of TGF-β3 promoting significantly higher levels of cartilage-specific extracellular matrix deposition. Altogether, these results demonstrate the potential of bioprinting sulfated bioinks as part of a 'single-stage' or 'point-of-care' strategy for regenerating cartilaginous tissues.

Statement of significance

This study highlights the potential of using sulfated interpenetrating network (IPN) bioink to support the regeneration of phenotypically stable articular cartilage. Construction of interpenetrating networks in the bioink enables unique high-fidelity bioprinting and provides synergistic increases in mechanical properties. The presence of alginate sulfate enables the capacity of high affinity-binding of TGF-β3, which promoted robust chondrogenesis *in vitro* and *in vivo*.

1. Introduction

Articular cartilage (AC) is a soft tissue lining the ends of bones in our joints, with limited intrinsic regenerative capacity due to its avascular nature [1,2]. Consequently, even minor lesions in AC cause pain, impaired mobility and can further develop to joint degeneration and osteoarthritis [3–5]. While current cell-based therapies [6–8], such as autologous chondrocyte implantation, are reported as promising, the limited availability of primary chondrocytes and their tendency to dedifferentiate during expansion may limit the widespread clinical adoption of such techniques [9,10]. This has motivated the development of innovative tissue engineering strategies to regenerate cartilaginous tissues and prevent the

* Corresponding author.
E-mail address: kellyd9@tcd.ie (D.J. Kelly).

https://doi.org/10.1016/j.actbio.2021.04.016

progression of joint diseases [11–14]. Three-dimensional (3D) bioprinting is an emerging technology capable of engineering geometrically complex implants that mimic specific aspects of native tissues through the simultaneous deposition of cell containing bioinks and supporting biomaterials in defined locations [15–19]. While this approach holds great potential in the field of tissue engineering and regenerative medicine, its progress has been limited by the lack of suitable bioinks that not only enable high fidelity bioprinting, but also provide appropriate biophysical and biochemical cues to promote a desired cellular phenotype and associated tissue development both *in vitro* and *in vivo*.

Hydrogels such as gelatin, alginate, hyaluronic acid and fibrin have been intensively explored as bioinks due to their biocompatibility and structural similarity to native extracellular matrix (ECM) [20–24]. While a range of natural hydrogels have been shown to support chondrogenesis *in vitro* [25,26], a major limitation of such biomaterials for cartilage tissue engineering is their weak mechanical strength and poor elasticity, making them unsuitable for load bearing applications *in vivo* until substantial new tissue accumulation has occurred. To this end, the ideal scaffold or hydrogel would possess mechanical properties approaching those of native articular cartilage, whilst still supporting chondrogenesis. Recently, there has been increased interest in the development of interpenetrating networks (IPN) hydrogels, consisting of two different polymers that are mixed with one another at the molecular scale, providing synergistic increases in compressive stiffness and toughness compared to the individual components of the network [27,28]. However, it is still challenging to develop an IPN bioink that provides both the necessary printing shape fidelity and the chondro-inductivity for cartilage bioprinting applications. This is particularly important for putative 'single-stage' or 'point-of-care' bioprinting strategies, where it is envisioned that constructs will be implanted following the printing process without any further *in vitro* maturation. Such a challenge could potentially be addressed by the development of IPN bioinks that are capable of delivering regulatory cues such as growth factors (GFs) with the capacity to direct progenitor/stem cell differentiation *in vivo* [29,30].

A number of strategies have been developed to temporally and spatially control GF delivery to modulate MSC differentiation [31–35]. These strategies, such as the covalent binding of GFs and the loading of GFs into microspheres, have demonstrated the capacity to control the release of GFs, however concerns related to initial burst releases and alternations to GF bioactivity remain. The observation that soluble GFs are bound to sulfated glycosaminoglycans (GAGs) *via* electrostatic interactions within the natural extracellular matrix (ECM) has motivated the use of sulfated biomimics to achieve controlled and sustained GF release [36,37]. Recently, scaffolds composed of sulfated polysaccharides have been shown to support strong binding affinity to multiple heparin-binding proteins, while retaining the characteristics of polysaccharides as supportive cell vehicles [38–42]. Therefore, the incorporation of sulfated GAG mimics into a hydrogel, to form a bioactive bioink, offers a promising approach for localized and sustained delivery of GFs to cells encapsulated within bioprinted implants targeting the repair of soft tissues.

The overall aim of this study was to develop a new class of alginate sulfate functionalized, growth factor eluting, alginate-gelatin methacryloyl (GelMA) IPN bioink capable of promoting chondrogenesis of encapsulated MSCs while simultaneously providing mechanical properties compatible with articular cartilage regeneration, as schematically shown in Fig. 1. Alginate and GelMA were selected to form IPN hydrogels due to their biocompability and suitability for the bioprinting of musculoskeletal tissues [23,34]. Additionally, alginate sulfate was synthesized and incorporated into the IPN, forming a sulfated IPN bioink (S-IPN) to improve the binding affinity with GFs. The printability, rheological and mechanical properties of the S-IPN bioink were first assessed. Next, the capacity of the S-IPN bioink to function as a delivery system for TGF-β3, a known chondrogenic growth factor, was evaluated. Finally, the chondro-permissiveness of the S-IPN bioink with affinity bound TGF-β3 was investigated *in vitro* and *in vivo* with the aim of assessing its potential as a putative 'off-the-shelf' or 'single-stage' strategy for articular cartilage repair.

2. Materials and methods

2.1. Cell isolation and expansion

Bone marrow derived mesenchymal stem cells (MSCs) were isolated from the femoral shaft of a 3-month old porcine purchased from a local abattoir within 3 hours of sacrifice and expanded in high glucose dulbecco's modified eagle's medium (hgDMEM, GlutaMAXTM; Bioscience, Ireland) supplemented with 10% fetal bovine serum (FBS, Biosciences, Ireland), 1% penicillin (100 U/ml)-streptomycin (100 µg/ml) (Biosciences, Ireland) hereafter, named XPAN. Following colony formation, MSCs were trypsinized and resuspended for a further passage at a density of 875,000 cells/T175 flask, 5 ng/mL fibroblast growth factor-2 (FGF-2, PeproTech EC, Ltd. UK) was added to the XPAN media which was changed twice weekly. All cell expansion was conducted in hypoxic conditions (5% O_2) and cells were used at passage 3. Tripotentiality was confirmed prior to use as previously described [43].

2.2. Preparation of alginate sulfate and gelatin methacryloyl (GelMA)

The sulfation of alginate was performed as described previously [41]. Briefly, 0.6 g alginate (LVG, Pronova, NovaMatrix DuPont, MW = ~75 kDa) was dissolved at 0.2% (w/v) in deionized water at 4 °C. Then 20 g of Dowex-X8 ion exchange resin (100-200 mesh, H^+ form, Sigma-Aldrich, Ireland) was added to the alginate solution and stirred for 30 mins. After the mixing, the supernatant was collected by centrifugation and the pH of the solution was adjusted to ~ 6.0 by dropwise addition of tributylamine (TBA, Sigma-Aldrich, Ireland) into the solution. The solution was then filtrated and lyophilized to obtain TBA-alginate. For sulfation of alginate, 0.6 g TBA-alginate was resuspended in 200 ml dimethylformamide with 6 g of sulfuric acid, followed by adding 12 g of N, N'-dicyclohexylcarbodiimide (Sigma-Aldrich, Ireland) and stirred for 2 h at room temperature. At the end of reaction, the precipitate was removed by filtration and the supernatant was mixed with three equal volumes of dichloromethane (Sigma-Aldrich, Ireland), resulting in a second precipitate. These precipitates were further dissolved in 0.5 N sodium hydroxide (Sigma-Aldrich, Ireland), the supernatant was obtained by filtration. The solution was then dialyzed against deionized water for 3 days and lyophilized to obtain the alginate sulfate. The degree of sulfation of the final products was 3 according to previous report [43]. Fourier transform infrared (FTIR) spectra of the alginate sulfate were recorded using a Spectrum 100 FT-IR spectrometer (PerkinElmer, Waltham, USA) in attenuated total internal reflection mode, the spectra were scanned between 500 and 400 cm^{-1}. Carbon-13 nuclear magnetic resonance (^{13}C NMR) were performed by NMR spectroscopy (400 MHz, Bruker Avance II 600 NMR, Switzerland) at ambient temperature.

To synthesis GelMA, methacrylic anhydride (1 mL per gram of gelatin) was added dropwise to 10 % (w/v) solution of gelatin (type A, from porcine skin, Sigma-Aldrich, Ireland) in PBS under constant stirring. After the reaction at 50 °C for 4 h, GelMA solution was diluted with 4 times volume of PBS and then dialyzed using dialysis tubes (12-14 kDa molecular weight cutoff, Spectrum Labs) in distilled water for 7 days at 40 °C to remove methacrylic acid and anhydride. Afterward, the solution was filtered using a filter with a

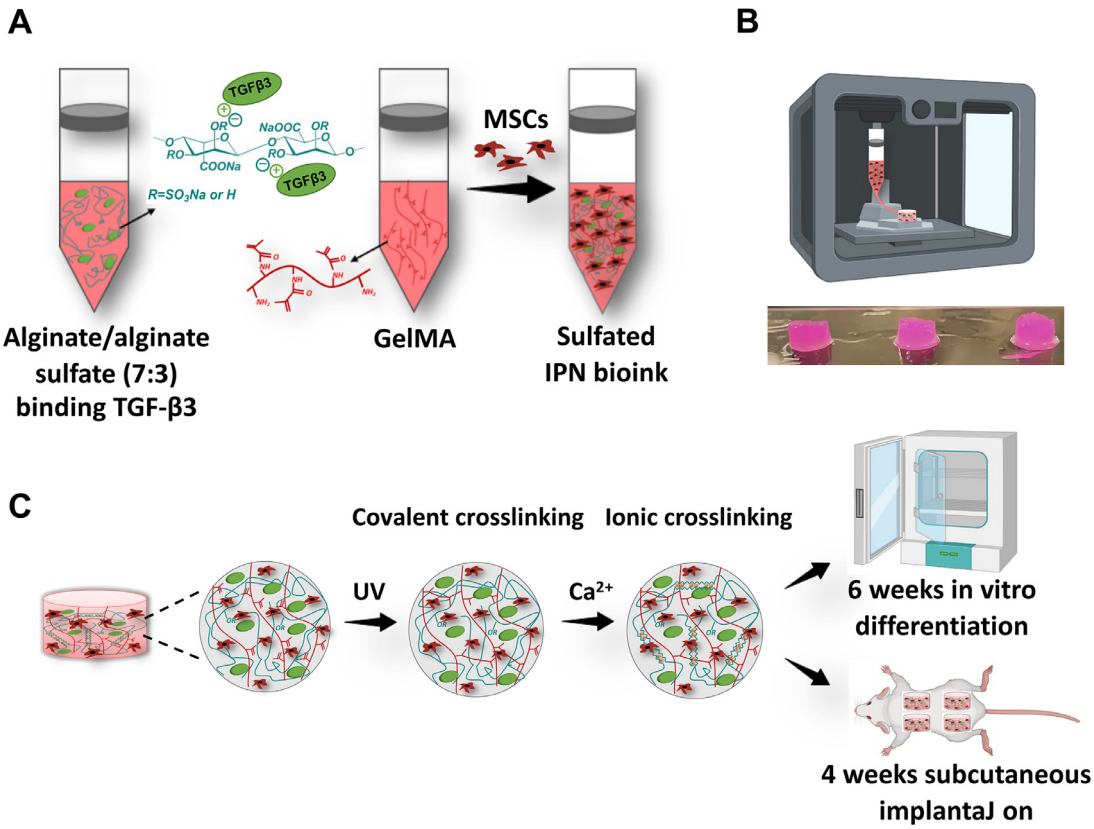

Fig. 1. Schematic representation of the sulfated interpenetrate network bioink preparation and printing process. (A) Illustration of preparing alginate/alginate sulfate-GelMA IPN bioink. Growth factor TGF-β3 was firstly affinity-bound to alginate/alginate sulfate, then blended with GelMA solution and porcine MSCs. (B) Image of 3D bioprinted constructs. (C) Schematic of crosslinking processes. Cylinders were printed and crosslinked under UV for 15 mins followed by ionic crosslink for another 15 mins in calcium bath. The constructs were either cultured *in vitro* for 6 weeks or subcutaneously implanted for 4 weeks.

pore size of 0.22 µm. Finally, the solution was lyophilized to obtain dry GelMA and stored at −20 °C before use.

2.3. Preparation of bioinks

Alginate, alginate sulfate and GelMA were dissolved separately in high glucose DMEM. Photoinitiator Irgacure 2959 (Sigma-Aldrich, Ireland) was solubilized in PBS and stored in the dark. To prepare IPN bioink, different components were mixed thoroughly at 37 °C in a volume ratio of alginate/GelMA/photoinitiator (4.5:4.5:1) using a dual syringe approach to get a solution consisting of 2% w/v alginate, 20% w/v GelMA and 0.1% w/v photoinitiator. The solution was next combined with MSCs in DMEM in a 1:1 volume ratio to yield IPN bioinks with a final concentration of 1% w/v alginate, 10% w/v GelMA, 0.05% w/v photoinitiator and 20 × 10^6 cells/ml. For rheological and mechanical characterization, the solution was mixed with DMEM without cells to get the same concentration. For S-IPN bioinks, alginate/alginate sulfate (7:3 v/v ratio) was used instead of using alginate solution alone. Three other inks, 1 % w/v alginate, 1 % w/v alginate/sulfated alginate and 10% w/v GelMA, were also prepared as controls.

2.4. Mechanical characterization

Cylindrical constructs (5 mm diameter and 5 mm height) were fabricated by casting inks into custom designed molds (3 % w/v agarose), followed by crosslinking under UV light (365 nm, 5 mW/cm^2. Uvitec, Cambridge UK) for 15 mins and further crosslinked in 50mM calcium chloride bath for 15 mins. All mechanical tests were performed using a standard material testing machine (Zwick Roell Z005) with a 5 N load cell. Briefly, constructs were kept hydrated in PBS bath maintained at room temperature. Stress tests were performed with an unconfined ramp compression to 50 % strain at a rate of 1 mm/s. The compression modulus was assessed from the initial linear region of the obtained stress-strain curves. To determine the elasticity of the constructs, samples were subjected to five compression cycles with strain amplitude of 10, 20, 30, 40 and 50% in sequence. Constructs permanent deformation (PD) after 5 cycles was calculated as follows: PD = (Test Speed * Δt)/h_0, where Δt is the interval of time at the start of the 5th cycle in which no force is applied to the sample, while h_0 is the initial height of the sample [44].

2.5. Scanning electron microscopy

The morphology of constructs were visualized using scanning electron microscopy (SEM, Zeiss Sigma 300) at 10 kV. The constructs were frozen in liquid nitrogen followed by lyophilization at -10 °C for 24 h. The dried constructs were then cut and sputter coated with 10 nm of gold before observation. The pore sizes were measured from SEM images using ImageJ software.

2.6. Swelling kinetics

The swelling behavior of constructs was assessed based on the following steps. The constructs were first lyophilized and dry weights (W_d) were recorded. Then, the samples were immersed in DMEM and incubated at 37 °C for 24 h. Swollen hydrogels were removed and weights were measured (W_s). The swelling ratio (SR) was calculated according to the following equation:

$$SR = (W_s - W_d)/W_d \quad (1)$$

2.7. Release kinetics of TGF-β3

The bioinks were prepared in DMEM as described above, and mixed with human Transforming Growth Factor-β3 (TGF-β3, PeproTech EC, Ltd. UK) using a dual-syringe approach, with the amount of TGF-β3 (240 ng/construct) equivalent to that normally added to the chondrogenic media over the course of a 6 week culture. 1% alginate, 1% alginate/alginate sulfate and 10% GelMA solutions were also prepared and loaded with TGF-β3 as controls. Once the TGF-β3 was mixed thoroughly the solutions were casted into agarose (3 % w/v) molds, followed by dual crosslinking process as described above. The release kinetics of each construct were determined by incubation in 2 ml growth media at 37 °C in hypoxia (5% O_2). At designated time points, media was changed and 1 ml of supernatant was collected and frozen at -80 °C. The amount of TGF-β3 in the supernatant was evaluated with enzyme-linked immunosorbent assay (ELISA, DY243, R&D Systems) according to the manufacturer's protocol.

2.8. Rheological assessment of bioinks

The rheological properties of all the bioinks were evaluated using a rheometer (MCR 102, Anton Paar GmbH, Austria). 1 ml of different bioinks were placed between parallel plates with a diameter of 25 mm (PP25) and the gap between two plates was set to 0.7 mm for all the tests. To investigate the temperature-dependent viscosity of different bioinks, temperature sweep tests were performed from 37 °C to 10 °C with the shear rate maintained at 100 s^{-1}. Then the dynamic viscosity of different bioinks was assessed by using shear rate sweep from 0.1 s^{-1} to 1000 s^{-1} at 13 °C, the shear thinning behavior of the bioinks was further quantified by fitting the shear rate-viscosity plots with Power Law equation:

$$\eta = K\varphi^{n-1} \quad (2)$$

where η is the dynamic viscosity, φ is the shear rate, and K and n denote shear thinning coefficients. Finally, to assess the recovery of viscosity of bioinks, thixotropic tests were performed by fixing the shear rate at 100 s^{-1} for 20 s before a sudden drop to 1 s^{-1} with the temperature maintained at 13 °C to simulate the printing process. Viscosity trends were assessed as a function of time.

2.9. 3D bioprinting and MSC differentiation

Cylindrical constructs encapsulated with MSCs (20×10^6 cells/ml) were printed using the 3D Discovery bioprinting system (Regen HU, Switzerland) operated within a laminar flow hood to ensure sterility throughout the fabrication process. Bioinks were loaded into a syringe and centrifuged to remove any air bubbles, and then printed at 13 °C, using an extrusion pressure of 0.1 MPa, 8 mm/s translation speed and a 25 G needle. The printability of bioinks was first evaluated by measuring the spreading ratio, defined as the width of the filament divided by the diameter of the needle, as previously described [36]. For *in vitro* evaluation, cylindrical constructs with a build diameter of 5 mm and height of 3 mm were printed layer by layer using an orthogonal 90 degree angle round pattern. The constructs were then crosslinked under UV light (365 nm, 5 mW/cm^2) for 15 mins and further ionically crosslinked in a bath of 60 mM $CaCl_2$ for 15 mins. Constructs were cultured at 37 °C, under hypoxic conditions (5% O_2) for 3 or 6 weeks in chondrogenically defined media (CDM): hgDMEM, penicillin (100 U/ml), streptomycin (100 µg/ml), L-proline (40 µg/ml), sodium pyruvate (100 µg/ml), linoleic acid (4.7 µg/ml), L-ascorbic acid-2-phosphate (50 µg/ml), bovine serum albumin (1.5 mg/ml), dexamethasone (100nM), 1× insulin-transferrin-selenium (all from Sigma-Aldrich), and human TGF-β3 (10 ng/ml). Constructs loaded with TGF-β3 were not supplemented with TGF-β3 in chondrogenic media. Media changes were performed twice weekly for all the groups.

2.10. Live/dead confocal microscopy

Cell viability was assessed at day 1, 21 and 42 using a live/dead viability assay. Briefly, constructs were sliced in longitudinal direction and rinsed in sterile deionized water followed by incubation for 1 h in phenol free DMEM containing 4 µM ethidium homodimer-1 and 2 µM calcein AM (Bioscience, UK). After incubation, sections were rinsed again in deionized water and imaged with Leica SP8 confocal microscope, and the viability was quantified using ImageJ software.

2.11. In vivo subcutaneous implantation

All the animal protocols were approved by the the ethics committee of Trinity College Dublin and Health Products Regulatory Authority (HPRA). Four 8-week old BALB/c OlaHsd-Foxn1nu nude mice (Envigo, Oxford, UK) were anaesthetized using a mixture of xylazine (10 mg/kg) and ketamine (100 mg/kg) given subcutaneously before surgery. Once anaesthetized, 5 mg/kg carprofen was also administered subcutaneously. Two incisions were made in the skin slightly lateral to the spine of each animal and four subcutaneous pockets were created. Two different group of constructs (S-IPN and TGF-β3 loaded S-IPN construct) were bioprinted and subsequently implanted, as previously described [45]. Mice were sacrificed after 4 weeks implantation by CO_2 inhalation and the constructs were analysed histologically and biochemically.

2.12. Biochemical analysis

Biochemical analyses were performed to assess the DNA, sGAG, collagen content and calcium deposition at day 1, 21 and 42. Prior the biochemical assays, constructs were sliced in half, weight recorded and frozen at -80 °C for subsequent assessment. Sliced constructs were either enzymatically digested with papain (125 µg/ml) in cysteine HCl (5 mM), sodium acetate (0.1 M), ethylenediaminetetraacetic acid (EDTA) (50 mM) (all from Sigma-Aldrich, Ireland) at 60 °C under rotation (10 rpm) for 18 h. The samples were then incubated with sodium citrate (1 M) for 1 h for DNA, sGAG and collagen evaluation. Otherwise the samples were chemically digested with HCl (1 M) at 60 °C under rotation (10 rpm) for 18 hr for calcium content analysis. The DNA content was determined *via* a Bisbencimide Hoechst assay. The sGAG content was estimated using a dimethylmethylene blue (DMMB) dye-binding assay, with the pH of the DMMB adjusted to 1.35 to exclude any background absorbance. Collagen content was indirectly measured by determining the hydroxyproline content after acidic hydrolysis (hydroxyproline/collagen content ratio of 1:7.69 [46]), and finally the calcium content was quantified using the o-cresolphthalein complexone method. All the contents at day 1 except collagen were subtracted from day 21 and 42 values for data presentation purposes.

2.13. Histological and immunohistochemical analysis

Histological analyses were carried out as previously reported [33]. Briefly, constructs were fixed in 4% paraformaldehyde overnight, followed by dehydrating, wax embedding and sectioning (6 µm slices). Sections were stained with picrosirius red for evaluating collagen distribution, aldehyde fuchsin/ alcian blue to assess sGAG content and alizarin red for visualizing calcium accumulation. Collagen type I, II and X were evaluated on sections using a standard immunohistochemical techniques, as previously reported [47].

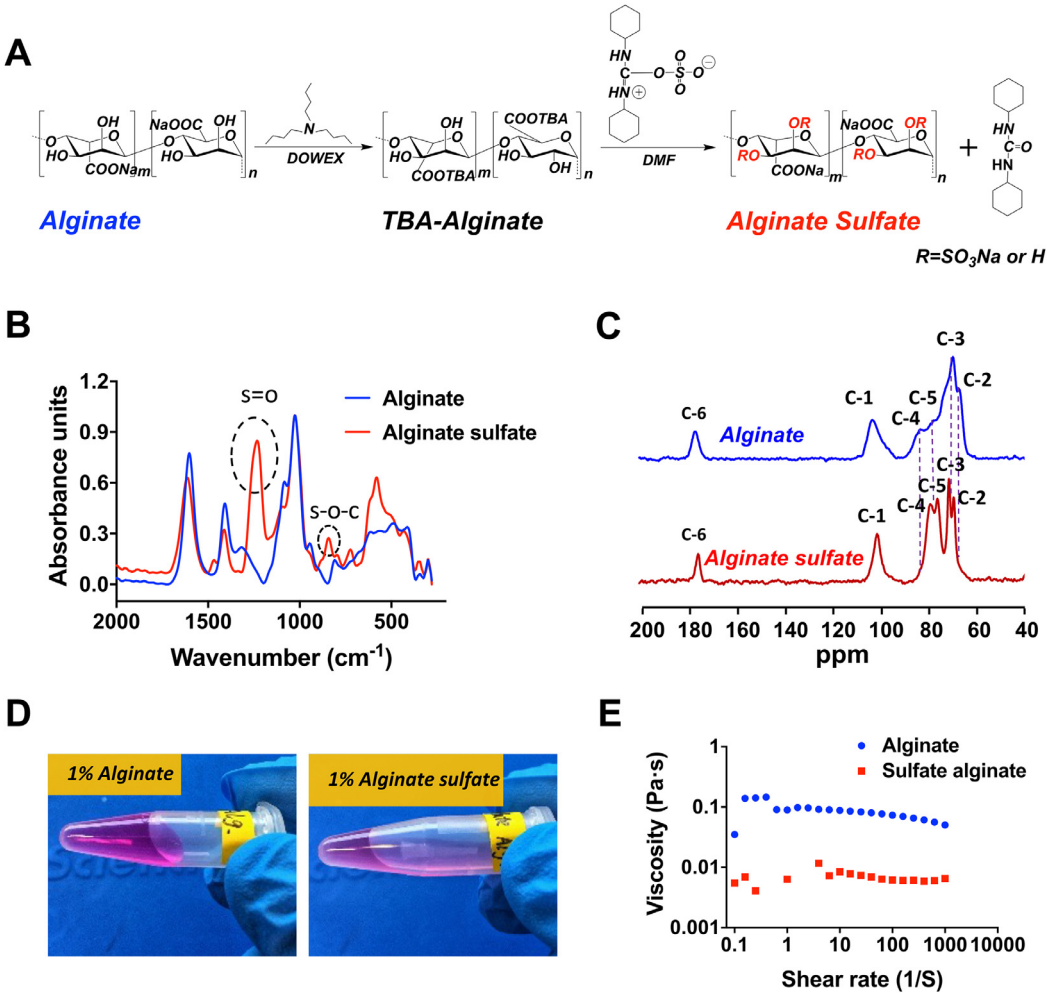

Fig. 2. Characterization of alginate sulfate. (A) Reaction scheme of the sulfation of uronic acids in alginate. (B) FTIR spectra of alginate sulfate and raw alginate. The new major peak at 1253 cm^{-1} was assigned to S=O asymmetric stretching and that at 843 cm^{-1} to symmetrical S-O-C vibration. (C) ^{13}C NMR spectra of alginate sulfate and raw alginate. (D) Images of 1% alginate and 1% alginate sulfate dissolved in DMEM medium. (E) Viscosity of 1% alginate and 1% alginate sulfate in the presence of shear rate in the range of 0.1 to 1000 s^{-1} at a frequency of 1 Hz.

2.14. Statistical analysis

All statistical analyses were performed using GraphPad Prism software. Numerical results were presented as mean ± standard deviation. Experiment groups were analyzed using a general linear model for analysis of variance followed by Tukey's test for multiple comparisons. Significance was accepted at a level of $p<0.05$.

3. Results

3.1. Sulfation and characterization of alginate

Alginate sulfate was synthesized by conversion of sodium alginate to a tertiary amine salt and followed by o-sulfation with carbodiimide and sulfuric acid, as schematically shown in Fig. 2A. Fig. 2B depicts the FTIR spectra of alginate and its sulfated form. The spectrum of alginate sulfate reveals two new characteristic absorption bands at 1253 $cm^{-1}$and 843 cm^{-1}, which corresponded to S=O asymmetric stretching and symmetrical S-O-C vibration respectively [48]. Sulfation of the uronic acid in alginate was further substantiated by ^{13}C NMR analyses (Fig. 2C). The two spectra reveal the matched chemical shifts of C-6 and C-1 at 174.8 and 100.1 ppm. The chemical shifts of C-4 and C-5 moved to a higher-field position after sulfation, from 82.1 to 77.8 ppm and 77.5 to 74.7 ppm respectively, whilst C-3 and C-2 shifts moved to lower-field positions in the spectrum of alginate sulfate, in agreement with previous studies [48,49].

After sulfate modification, the viscosity of the alginate decreased significantly (Fig. 2D). A rheology test to characterize viscosity as a function of shear rate was performed and quantitatively confirmed the dramatic decrease of viscosity of the 1% alginate sulfate solution compared to that of unmodified 1% alginate (Fig. 2E).

3.2. Rheological properties and 3D printability of bioinks

The rheological characteristics of the IPN bioinks were next examined, including temperature dependence of viscosity, shear thinning behavior and thixotropic property, as compared to individual components of the IPN. For all GelMA containing bioinks, that is the 10% GelMA, IPN and S-IPN inks, the temperature sweep analysis indicates that the viscosity increased dramatically when the temperature dropped below 20 °C (Fig. 3A). Additionally, the temperature at which the viscosity abruptly increased was higher in the IPN and S-IPN bioinks (~20 °C and 18 °C, respectively) compared to that of 10% GelMA only (~15 °C). However, in the case of 1% alginate and 1% alginate/alginate sulfate solutions, there was no obvious variation in viscosity with changes in temperature. On the

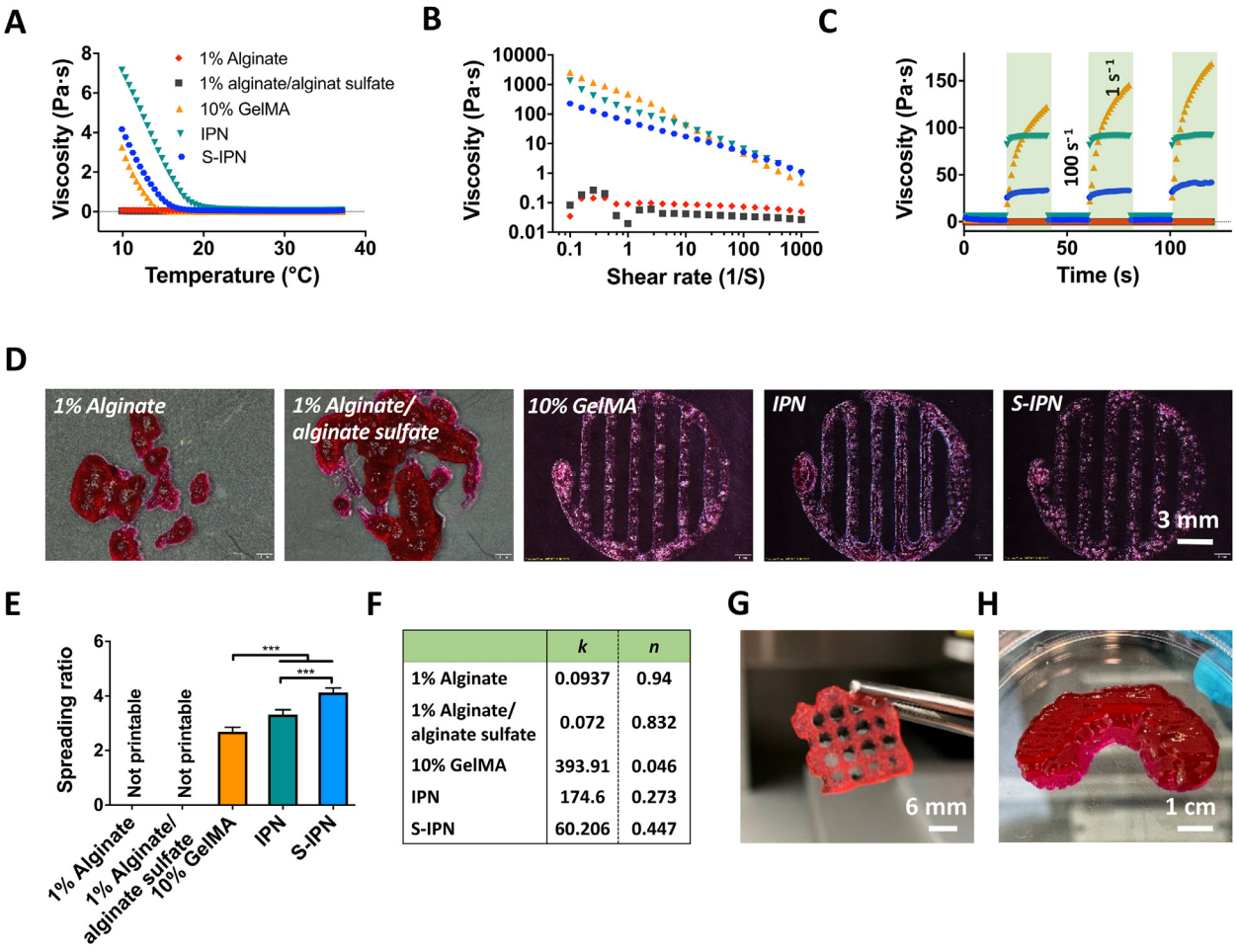

Fig. 3. Rheological properties and 3D-printability of 1% alginate, 1% alginate/alginate sulfate, 10% GelMA, IPN and S-IPN bioinks. (A) Viscosity of bioinks as a function of temperatures changing from 37 to 10 °C. (B) Viscosity of different bioinks in the presence of shear rate in the range of 0.1 to 1000 s^{-1} at a frequency of 1 Hz. (C) Viscosity recovery test of the bioinks subjected to a shear rate varying between 1 and 100 s^{-1} for 20 s, mimicking the 3D printing process. (D) Printed hydrogels in a defined pattern generated using different bioinks. (E) Post printing spreading ratio (width of filament divided by needle diameter). n = 4, ***p < .001. (F) Values of shear thinning coefficients of the bioinks derived by fitting the Power Law Eq. (2) to the liner region of the shear rate-viscosity plots in Fig. 3B. (G, H) Printed 3D lattice and meniscus implant using S-IPN bioink.

basis of these results and pilot printing tests, a constant temperature of 13 °C was chosen in order to ensure the printability of the inks.

The shear-dependent viscosity of the different bioinks was acquired from shear rate sweep measurements (Fig. 3B). Shear-thinning behavior was observed for all GelMA containing bioinks at 13 °C, characterized by a continuous decrease in viscosity with increasing shear rate, with the 10% GelMA only bioink displaying more obvious shear-thinning behavior compared to the IPN and S-IPN bioinks, with a sharper shear rate-viscosity profile. On the other hand, alginate based bioinks without pre-crosslinking did not display shear thinning behavior, suggesting such pure alginate based bioinks would be associated with poor shape fidelity when bioprinting.

The characterization of thixotropic properties was also performed under alternating high/low shear rates (100 or 1 s^{-1}) to simulate the bioprinting process [50]. IPN and S-IPN bioinks went from fluid-like to solid-like behavior in response to applied shear rates, whereas the viscosity of 1% alginate and 1% alginate/alginate sulfate solutions remained constant over the test (Fig. 3C). Additionally, compared to 10% GelMA, the responses to shear rate changes were rapid and repeatable in IPN and S-IPN bioinks, indicative of highly thixotropic behavior, which is essential for extrusion-based bioprinting.

The printability and shape fidelity of the bioinks were further confirmed by characterization of the filament spreading ratio (ratio of the width of deposited filaments to the needle diameter) after deposition (Fig. 3D and E). Generally, continuous filaments were printed with uniform size in the case of 10% GelMA, IPN and S-IPN bioinks, with the lowest spreading ratio (2.73 ± 0.25) was measured in 10% GelMA bioinks, indicating the best printability. In contrast, alginate only bioinks were completely unprintable; these bioinks dispersed upon extrusion, probably due to their low shear viscosity (Fig. 3B). These results were in good agreement with the analysis of bioink shear thinning properties. By fitting the Power Law model in the form of Eq. (2) to shear rate-viscosity flow curves, the degree of shear thinning behavior of the bioinks was quantified (Fig. 3F). The consistency coefficient (K) is the viscosity of the bioinks at a shear rate of 1 s^{-1}. The flow behavior index (n) expresses how non-Newtonian a bioink is, with n approaching 0 indicating higher shear thinning of the bioink [51]. To further demonstrate the print fidelity of the S-IPN bioink, grid-like structures and anatomically sized constructs mimicking a sheep meniscus were successfully printed with high fidelity (Fig. 3G and H).

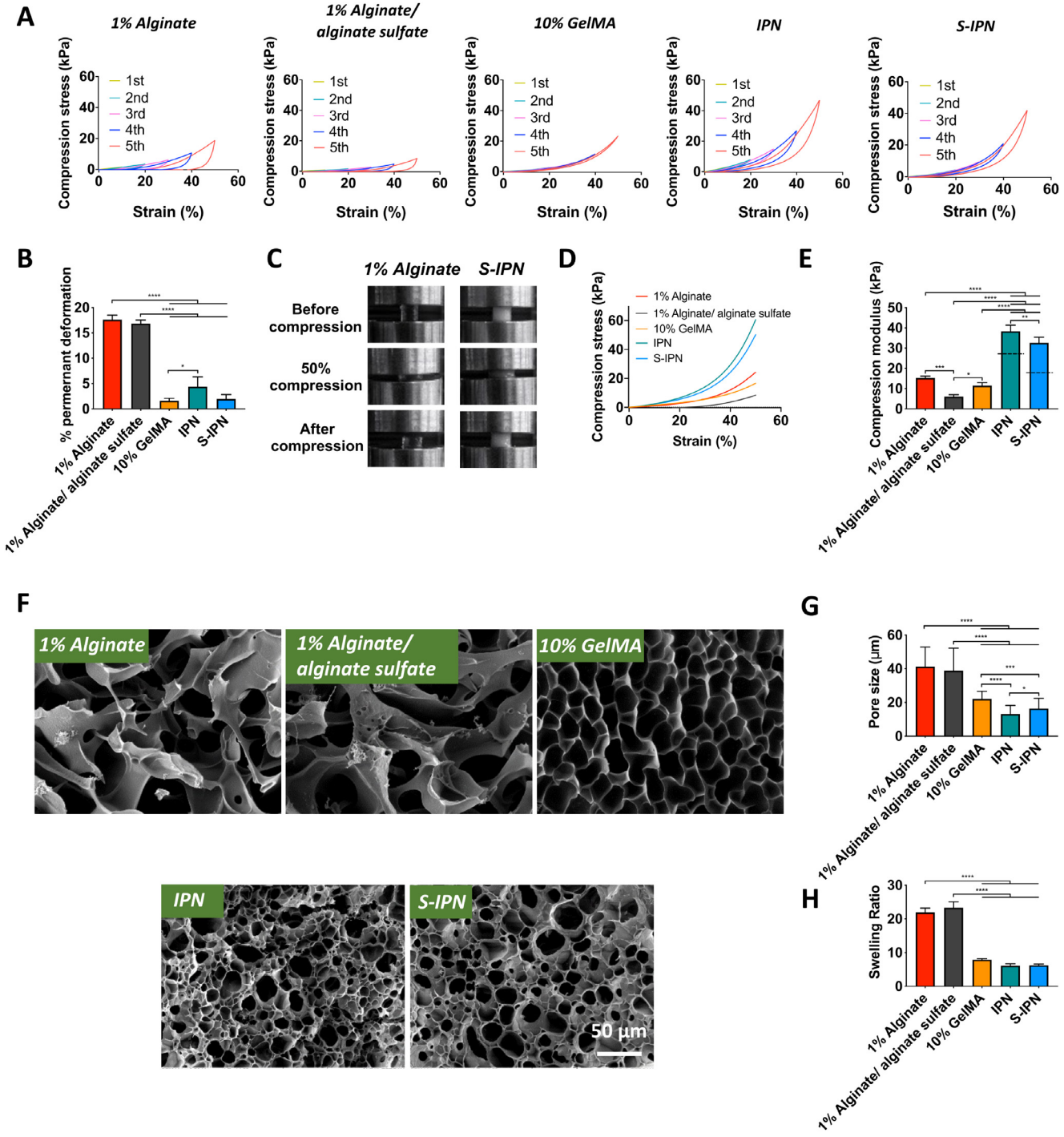

Fig. 4. Mechanical properties of the constructs. (A) Stress-strain hysteresis plots of 1% alginate, 1% alginate/alginate sulfate, 10% GelMA, IPN and S-IPN constructs for 5 cycles of compression. Strain increased by 10% increments with each cycle from 10% to 50%. (B) Permanent deformation of constructs after cyclic compression. n = 3. (C) Representative images of cylindric 1% alginate and S-IPN constructs before, during and after being compressed to 50% strain. (D) Compression stress-strain curves of constructs from each group. (E) Compression modulus of the constructs derived from the linear region of compressive strain-stress curves. Dash line represents the sum of single components. n = 4. (F) SEM images of porous structures of each hydrogels after crosslinking. (G) Pore size of hydrogels, n = 3 with over 30 pores measured for each sample. (H) Swelling ratio of freeze dried constructs after 24 hours incubation in DMEM. n = 3, $^{*}p \leq .05$, $^{**}p \leq .01$, $^{***}p \leq .001$, and $^{****}p \leq .0001$.

3.3. Interpenetrating networks provide synergistic increases in mechanical properties to printed constructs

The mechanical properties of the S-IPN constructs were evaluated by unconfined compression tests and compared to single component samples. Constructs were first subjected to cyclic compression tests, which consisted of five cycles with increasing strain amplitude from 10% to 50%, in order to characterize their elastic properties. Ionically crosslinked networks (1% alginate and 1% alginate/alginate sulfate) exhibited pronounced hysteresis and significant plastic deformation (above 16% of the initial height) after 5 cycles of loading and unloading, while 10% GelMA showed high resilience with only 1.60 ± 0.48% permanent deformation measured (Fig. 4A and B). The dual crosslinked constructs (IPN and S-IPN) were also shown to be resilient under cyclic loading, particularly the S-IPN which exhibited negligible hysteresis and was able to

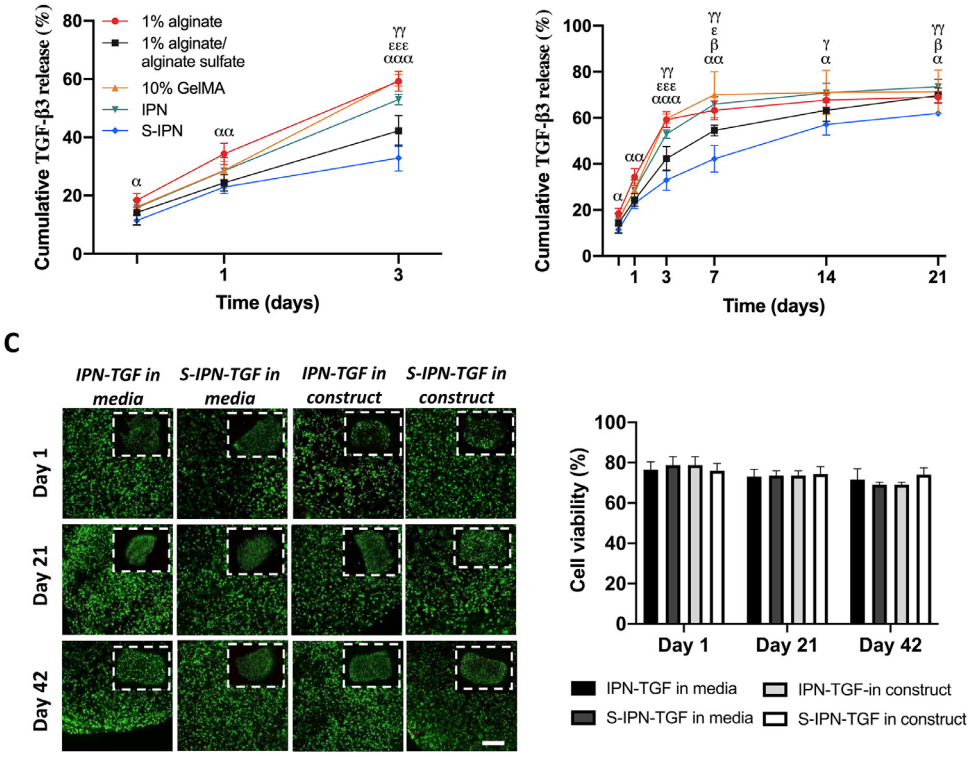

Fig. 5. TGF-β3 release and cell viability within printed constructs. (A, B) TGF-β3 release profiles from constructs within first 3 days and up to 21 days of culture assessed using an ELISA assay. n = 4, α, β, ε and γ=statistical significance *via* two-way ANOVA test of S-IPN vs 1% alginate, 1% alginate/alginate sulfate, 10% GelMA and IPN, respectively. (C) Representative images of live/dead staining of MSCs within constructs at various time points (day 1, 21, and 42) throughout the culture duration. The main images show high magnification images of the constructs. The inset images show the full constructs. Green and red indicate live and dead cells, respectively. Scale bar: 300 µm. (D) Quantification of cell viability in 3D-printed constructs. 3 samples for each group analysed.

recover to its original shape with slight permanent deformation (1.96 ± 0.87%). Furthermore, the S-IPN construct withstood 50% compressive strain and fully recovered after unloading, whereas 1% alginate showed noticeable plastic deformation (Fig. 4C), demonstrating again the highly elastic nature of the S-IPN constructs. Moreover, the mechanical strength of the S-IPN constructs was greatly enhanced compared to that of single component constructs (Fig. 4A), which was further confirmed by ramp compression testing (Fig. 4D and E). The results revealed that the dual crosslinked S-IPN constructs (32.48 ± 4.23 kPa) had a 5-fold higher compressive modulus than 1% alginate/alginate sulfate hydrogel (6.85 ± 1.17 kPa) and 3-fold higher compressive modulus than 10% GelMA alone (11.07 ± 1.92 kPa). Additionally, the compression modulus of S-IPN constructs was significantly higher than the sum of the individual components, indicating a synergistic effect of dual crosslinking on construct stiffness.

Scanning electron microscopy (SEM) observation revealed that both the IPN and S-IPN constructs had highly interconnected porous structures with an average pore size of around 20 µm, which was smaller than single component hydrogels, presumably due to the interpenetrating network generated from the dual crosslinking process (Fig. 4F, G). The swelling behavior of all combinations of hydrogels was also investigated (Fig. 4H), with the 1% alginate and 1% alginate sulfate hydrogels displaying significantly higher swelling properties than the IPN and S-IPN constructs.

3.4. Sulfation of alginate slows TGF-β3 release

In order to investigate the capacity of the sulfated IPN bioink to bind, trap and release growth factors, gel precursor solutions were loaded with TGF-β3 and the release kinetics were monitored by ELISA. There was an initial burst release of TGF-β3 from the 1% alginate, 10% GelMA and IPN (approximately 60%) occurring within the first three days of culture, whereas alginate sulfate incorporated hydrogels, particularly the S-IPN, showed a more sustained initial release (Fig. 5A). Over the entire test period, 1% alginate and 10% GelMA hydrogels displayed similar release profiles, with the majority of TGF-β3 released by day 7, followed by a plateau up to day 21 (Fig. 5B). At 7 days, the cumulative TGF-β3 release from the IPN constructs was 65.9 ± 3.8% compared to value of 42.2 ± 5.8% for the S-IPN. Moreover, a sustained release of growth factor over 21 days was observed for the S-IPN, demonstrating the high affinity between alginate sulfate and TGF-β3.

3.5. A S-IPN bioink containing TGF-β3 promotes chondrogenesis of MSCs in vitro

Having demonstrated the capacity of the S-IPN hydrogel to control the release of TGF-β3, we next sought to explore the potential of the S-IPN bioink as a delivery system for chondrogenic growth factors to promote chondrogenesis of MSCs *in vitro*. Cylinder constructs were 3D bioprinted using cell laden IPN and S-IPN bioinks with or without encapsulated TGF-β3. One day after printing, a live/dead assay was performed on the constructs, demonstrating limited cell death in all groups (Fig. 5C). In addition, cell viability was maintained at approximately 80% throughout the culture duration (Fig. 5D). Moreover, it can be seen that cells were homogenously distributed in all the constructs. These MSC-laden 3D printed constructs were then cultured under identical conditions *in vitro* for 42 days and the chondrogenic differentiation of the encapsulated cells was assessed histologically and biochemically. All the constructs stained intensely for picrosirius red and collagen type II, while more pronounced aldehyde fuchsin/alcian blue staining was observed in TGF-β3 loaded S-IPN constructs at day

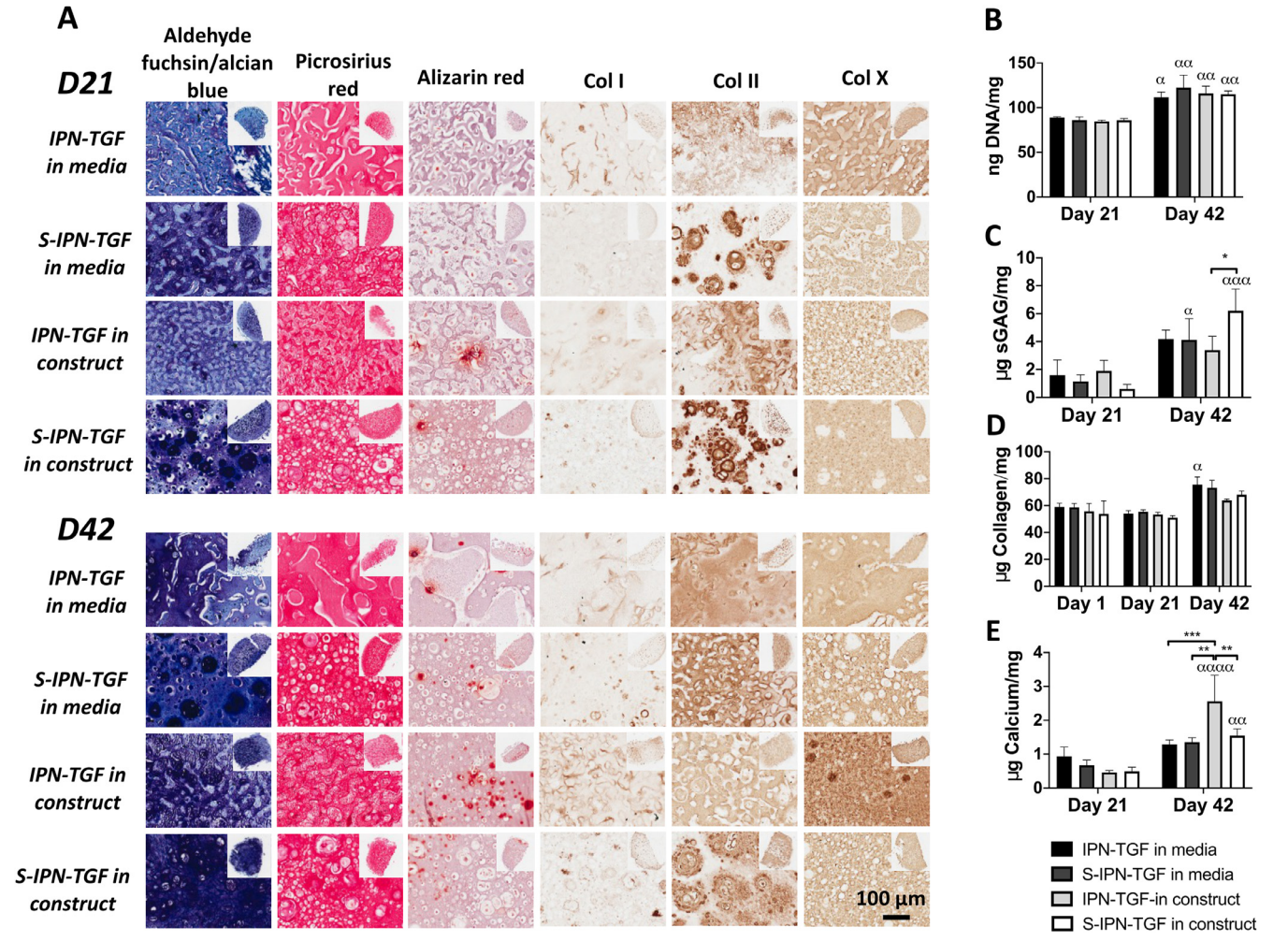

Fig. 6. ***In vitro*** **chondrogenesis evaluation of IPN and S-IPN constructs with TGF-β3 either in culture media or construct**. (A) Histological and immunohistochemical staining for sulphated glycosaminoglycan (sGAG), collagen, calcium, collagen type I, collagen type II and collagen type X deposition at day 21 and 42 of culture. (B-E) Quantification of DNA, sGAG, collagen and calcium deposition in each construct. n = 3, $^{*}p \leq .05$, $^{**}p \leq .01$, and $^{***}p \leq .001$. $^{\alpha}p < .05$, $^{\alpha\alpha}p \leq .01$, $^{\alpha\alpha\alpha}p \leq .001$ and $^{\alpha\alpha\alpha\alpha}p \leq .0001$ vs. day 21 of the same bioink.

42, indicating a greater level of sGAG accumulation (Fig. 6A). This was confirmed by quantitative biochemical analysis of the resultant tissue, which demonstrated that collagen and sGAG accumulation increased over culture time in all constructs, with significantly more sGAG synthesized in the TGF-β3 loaded S-IPN constructs at day 42 (Fig. 6C and 6D). Negligible alizarin red staining, a marker of mineralization, was found in IPN and S-IPN constructs at day 21 when TGF-β3 was supplied to the media, with some very small pockets of mineral deposition observed by day 42. More importantly, within S-IPN-TGF constructs, no significant difference was found in terms of calcium deposition compared to constructs where TGF-β3 was continuously supplied to the media at both time points. In contrast, more intense staining was observed in the IPN-TGF constructs, particularly at day 42, as evident by a significant increase in calcium content (Fig. 6E). Immunohistochemical analysis revealed that all constructs stained weakly for collagen type I at all time points; however, stronger staining of collagen type X was observed within TGF-β3 loaded IPN constructs at day 42, suggesting the hypertrophic development of MSCs with this bioink.

3.6. A S-IPN bioink containing TGF-β3 promotes chondrogenesis of MSCs in vivo

We next sought to assess the potential of the TGF-β3 loaded S-IPN bioink to promote chondrogenesis *in vivo* in a subcutaneously implantation mouse model (Fig. 7A). To this end, the capacity of the S-IPN bioink encapsulated with TGF-β3 or the S-IPN bioink alone to promote cartilage formation was compared. After 4 weeks *in vivo*, S-IPN constructs supplemented with TGF-β3 resembled cartilage macroscopically (Fig. 7B). Histological analysis revealed that more matrix appeared to accumulate within the TGF-β3 loaded S-IPN constructs, with intense staining for sGAG and collagen type II. In contrast, S-IPN constructs without growth factor release demonstrated lower levels of sGAG and collagen type II staining (Fig. 7C), which were in agreement with biochemical evaluations. In addition, negligible alizarin red and collagen type X staining was found in the TGF-β3 loaded S-IPN constructs. These results demonstrate the potential of growth factor-releasing S-IPN bioinks to modulate MSC differentiation, supporting the development of a stable, hyaline-like cartilage tissue *in vivo*.

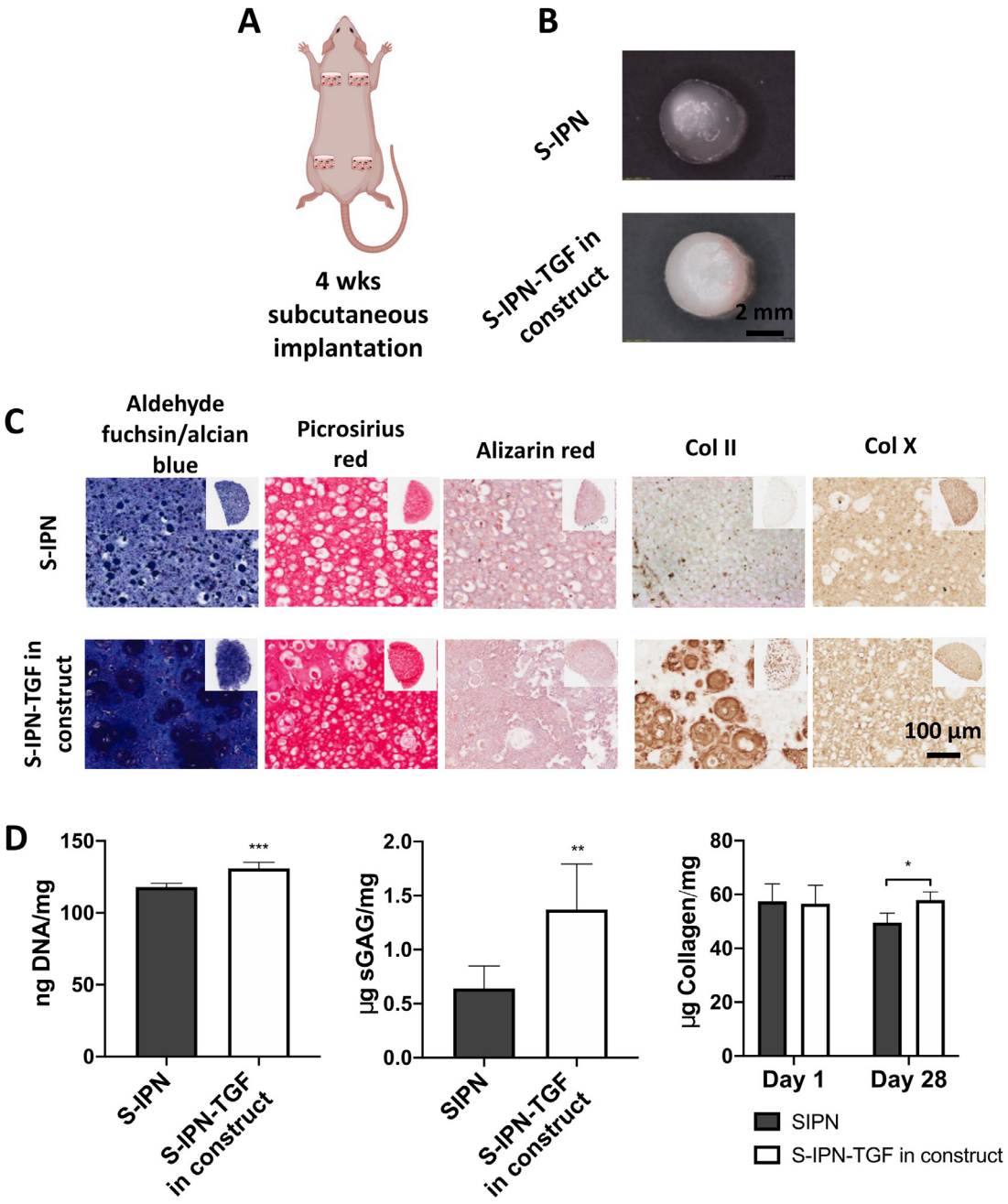

Fig. 7. Chondrogenesis evaluation of S-IPN constructs with TGF-β3 release *in vivo*. (A) Scheme of subcutaneous implantation of constructs. (B) Macroscopic view of S-IPN constructs with and without the incorporation of TGF-β3. (C) Histological and immunohistochemical staining for sGAG, collagen, calcium, collagen type II and collagen type X deposition after 4 weeks *in vivo*. (D) Quantification of DNA, sGAG, collagen and calcium deposition in each group. n = 5, $^{*}p \leq .05$, $^{**}p \leq .01$, and $^{***}p \leq .001$.

4. Discussion

This study described the development of a new class of sulfated IPN bioink and investigated its potential for delivering growth factors to encapsulated MSCs as a promising translational approach to generate articular cartilage. The IPN bioinks provided synergistic improvements in mechanical properties that translated into mechanically tough and resilient bioprinted tissues. Furthermore, the presence of alginate sulfate in the bioink enabled long-term sustained release of TGF-β3, which promoted robust and stable chondrogenesis of MSCs *in vitro*. In addition, implantation of TGF-β3 loaded printed S-IPN constructs directly post-printing was capable of driving chondrogenesis in a subcutaneous environment. Taken together, these findings open up the possibility of bioprinting and then directly implanting such TGF-β3 laden-sulfated IPN bioinks as part of a 'single-stage' strategy for cartilage regeneration.

The sulfated IPN bioink was found to exhibit good 3D printability and post-printing shape fidelity, which was identified as the primary requirement when developing bioinks, largely due to the physical gelation of GelMA during the printing process at a relatively low temperature. GelMA has been widely explored as a bioink to print complex tissues because of its high biocompability, elasticity and, more importantly, its thermo-dependent viscosity [52–54]. Here, IPN and S-IPN bioinks were found capable of depositing smooth filaments and complex large structures, despite their less pronounced shear thinning properties compared to that of GelMA only. This may be correlated to the effect of uncrosslinked alginate/alginate sulfate on relieving the entangle-

ment of GelMA chains, which in turn also resulted in more obvious thixotropic behavior of the IPN or S-IPN bioinks. Of note, it was found that the S-IPN bioink had relatively lower viscosity compare to the IPN bioink, despite the fact that only a small portion of alginate sulfate was used in the S-IPN bioink, which may be due to the low viscosity of sulfated alginate as shown in Fig. 1E. Indeed, other studies have demonstrated that after sulfation, the molecular weight of alginate decreased dramatically and hence may result in a significant decrease in viscosity [40,41], which could also explain the unprintability of a mixture of 10% GelMA and 1% alginate sulfate (data not shown here).

The mechanical properties of bioprinted constructs are crucial for maintaining structural integrity and, more importantly, withstanding mechanically loading once implanted *in vivo* [55,56]. Nevertheless, many bioprinted constructs using conventional single network hydrogel bioinks are mechanically weak and lack elasticity. In contrast, the sulfated IPN constructs developed in this study provide synergistic increases in mechanical properties compared to single component hydrogels, demonstrating the capability of withstanding severe mechanical deformation, which may be attributed to stress-sharing between the hydrogel networks and energy dissipation through reversible disruption of ionically crosslinked networks while covalently crosslinked networks remains intact. In addition, the swelling ratio of S-IPN constructs remained similar to that of the GelMA component, indicating negligible influence on nutrient transportation; this is generally not expected with more conventional methods for improving hydrogel mechanical properties, including increasing polymer concentration and enforcing with particles [57]. Of note is that in spite of the improvement of mechanical properties, the compressive modulus of the S-IPN constructs still remained at least one order of magnitude lower than that of native articular cartilage [28,58]. Further studies are therefore required to develop implants that better mimic the mechanical properties of native articular cartilage, for example by employing multiple-tool fabrication systems to reinforce bioinks with appropriately designed polymer frameworks [59].

To leverage the chondrogenic potential of the bioink, alginate sulfate was synthesized and incorporated to this system to facilitate sustained delivery of TGF-β3. It is well known that native ECM components, such as sulfated GAGs, have the capacity to bind growth factors [60]. However, previous studies in our lab have demonstrated that decellularized ECM has limited control on growth factors releasing, possibly due to the decellularization process which may remove sulfated GAGs [22,61]. In contrast, alginate, as a biocompatible natural polysaccharide, can be sulfated *via* chemical reaction to be negatively charged and, further, has been found capable of strong binding to over 10 (positively charged) heparin-binding proteins [41,62]. In this study, a mixture of alginate and sulfated alginate demonstrated the capacity to more strongly bind TGF-β3 compared to native alginate or GelMA alone. Furthermore, the S-IPN bioink supported greater growth factor retention and sustained release over at least 21 days of culture, as evident by the ELISA results (Fig. 5A and B).

The prolonged activity of the affinity-bound TGF-β3 led to robust and stable chondrogenesis of MSCs *in vitro*. The histological and biochemical findings demonstrated that a TGF-β3 eluting S-IPN bioink supported superior chondrogenesis compared to control IPN bioinks eluting TGF-β3. As previous studies have demonstrated that chondrogenically primed MSCs tend to further differentiate toward a hypertrophic phenotype [63,64], resulting in calcification of the engineered tissues, we also sought to assess the tendency of our bioprinted tissues to progress along an endochondral pathway. Progression along this pathway is a particular concern when engineered tissues are inefficiently primed along a chondrogenic pathway [65]. Encouragingly, no significant difference in calcium deposition and collagen type X accumulation was observed in the S-IPN groups, irrespective of whether TGF-β3 was encapsulated into the bioink or continuously supplemented into the media. In contrast, significantly higher levels of mineralization were found in the IPN constructs when TGF-β3 was encapsulated into the bioink. These findings may be explained, at least in part, by the prolonged activity of TGF-β3 in the sulfated bioink. In addition, the negatively charged alginate sulfate may repel the same negatively charged phosphate donors [66], suppressing hypertrophic calcification. In should be noted that no significant difference in the extent of chondrogenesis and tissue calcification was observed between the IPN and S-IPN bioinks when TGF-β3 was continuously supplemented into the media, suggesting a dominating role for the sustained release of TGF-β3 rather than the materials themselves in directing this process.

The chondro-inductive nature of the sulfated bioink with affinity-binding TGF-β3 was further confirmed *in vivo*, with significantly more cartilage ECM deposited after 4 weeks compared to a sulfated IPN bioink without exogenous TGF-β3. Importantly, negative staining for calcium and collagen type X deposition were found in the TGF-β3 loaded S-IPN constructs, indicating the development of hyaline-like cartilage *in vivo*. The limit change of collagen content compared to that of Day 1 was possibly due to the degradation of the GelMA *in vivo*, which may counteract the effect of collagen deposition by the encapsulated MSCs. Of note is that the constructs were subcutaneously implanted into nude mice immediately after bioprinting without any further *in vitro* culture. Taken together, these results provide further support for the concept of employing sulfated IPN bioinks as part of a ‘single-stage or ‘point-of-care’ strategy for articular cartilage regeneration.

5. Conclusion

In conclusion, these results highlight the potential of using sulfated IPN bioinks to support the regeneration of phenotypically stable articular cartilage. Construction of IPN bioinks provided synergistic increases in mechanical properties with improved toughness and elasticity. The presence of alginate sulfate supported high affinity-binding and sustained release of TGF-β3, which promoted robust chondrogenesis and also suppressed hypertrophy of encapsulated MSCs both *in vitro* and *in vivo*. Combining such sulfated IPN bioinks with multiple-tool fabrication systems holds great potential in the field of orthopedic medicine.

Declaration of Competing Interest

The authors declare that they have no known competing financial interests or personal relationships that could have appeared to influence the work reported in this paper.

Acknowledgments

Funding for this work was provided by the European Research Council (JointPrinting; ERC-CoG-2014-647004).

Supplementary materials

Supplementary material associated with this article can be found, in the online version, at doi:10.1016/j.actbio.2021.04.016.

References

[1] C. Chung, J.A. Burdick, Engineering cartilage tissue, Adv. Drug Deliv. Rev. 60 (2008) 243–262, doi:10.1016/j.addr.2007.08.027.
[2] K.P.H. Pritzker, S. Gay, S.A. Jimenez, K. Ostergaard, J.P. Pelletier, K. Revell, D. Salter, W.B. van den Berg, Osteoarthritis cartilage histopathology: grading and staging, Osteoarthr. Cartil. 14 (2006) 13–29, doi:10.1016/j.joca.2005.07.014.

[3] A.A. Pitsillides, F. Beier, Cartilage biology in osteoarthritis - lessons from developmental biology, Nat. Rev. Rheumatol. 7 (2011) 654–663, doi:10.1038/nrrheum.2011.129.
[4] T. Pap, A. Korb-Pap, Cartilage damage in osteoarthritis and rheumatoid arthritis - two unequal siblings, Nat. Rev. Rheumatol. 11 (2015) 606–615, doi:10.1038/nrrheum.2015.95.
[5] M. Lacourt, C. Gao, A. Li, C. Girard, G. Beauchamp, J.E. Henderson, S. Laverty, Relationship between cartilage and subchondral bone lesions in repetitive impact trauma-induced equine osteoarthritis, Osteoarthr. Cartil. 20 (2012) 572–583, doi:10.1016/j.joca.2012.02.004.
[6] C. Madeira, A. Santhagunam, J.B. Salgueiro, J.M.S. Cabral, Advanced cell therapies for articular cartilage regeneration, Trends Biotechnol. 33 (2015) 35–42, doi:10.1016/j.tibtech.2014.11.003.
[7] C. Loebel, J.A. Burdick, Engineering stem and stromal cell therapies for musculoskeletal tissue repair, Cell Stem Cell 22 (2018) 325–339, doi:10.1016/j.stem.2018.01.014.
[8] P. Vavken, D. Samartzis, Effectiveness of autologous chondrocyte implantation in cartilage repair of the knee: a systematic review of controlled trials, Osteoarthr. Cartil. 18 (2010) 857–863, doi:10.1016/j.joca.2010.03.005.
[9] D.J. Huey, J.C. Hu, K.A. Athanasiou, Unlike bone, cartilage regeneration remains elusive, Science (80-.) 338 (2012) 917–921, doi:10.1126/science.1222454.
[10] R. Mardones, C.M. Jofré, J.J. Minguell, Cell therapy and tissue engineering approaches for cartilage repair and/or regeneration, Int. J. Stem Cells. 8 (2015) 48–53, doi:10.15283/ijsc.2015.8.1.48.
[11] B.J. Huang, J.C. Hu, K.A. Athanasiou, Cell-based tissue engineering strategies used in the clinical repair of articular cartilage, Biomaterials 98 (2016) 1–22, doi:10.1016/j.biomaterials.2016.04.018.
[12] M. Bhattacharjee, J. Coburn, M. Centola, S. Murab, A. Barbero, D.L. Kaplan, I. Martin, S. Ghosh, Tissue engineering strategies to study cartilage development, degeneration and regeneration, Adv. Drug Deliv. Rev. 84 (2015) 107–122, doi:10.1016/j.addr.2014.08.010.
[13] K.-C. Li, Y.-C. Hu, Cartilage tissue engineering: recent advances and perspectives from gene regulation/therapy, Adv. Healthc. Mater. 4 (2015) 948–968, doi:10.1002/adhm.201400773.
[14] L. Jia, Y. Zhang, L. Yao, P. Zhang, Z. Ci, W. Zhang, C. Miao, X. Liang, A. He, Y. Liu, S. Tang, R. Zhang, X. Wang, Y. Cao, G. Zhou, Regeneration of human-ear-shaped cartilage with acellular cartilage matrix-based biomimetic scaffolds, Appl. Mater. Today. 20 (2020) 100639, doi:10.1016/j.apmt.2020.100639.
[15] A. Lee, A.R. Hudson, D.J. Shiwarski, J.W. Tashman, T.J. Hinton, S. Yerneni, J.M. Bliley, P.G. Campbell, A.W. Feinberg, 3D bioprinting of collagen to rebuild components of the human heart, Science (80-.) 365 (2019) 482–487, doi:10.1126/science.aav9051.
[16] I. Matai, G. Kaur, A. Seyedsalehi, A. McClinton, C.T. Laurencin, Progress in 3D bioprinting technology for tissue/organ regenerative engineering, Biomaterials 226 (2020) 119536, doi:10.1016/j.biomaterials.2019.119536.
[17] A.C. Daly, F.E. Freeman, T. Gonzalez-Fernandez, S.E. Critchley, J. Nulty, D.J. Kelly, 3D Bioprinting for cartilage and osteochondral tissue engineering, Adv. Healthc. Mater. (2017) 6, doi:10.1002/ADHM.201700298@10.1002/(ISSN)2192-2659.BIOFABRICATION-FOR-TISSUE-ENGINEERING.
[18] S. Ostrovidov, S. Salehi, M. Costantini, K. Suthiwanich, M. Ebrahimi, R.B. Sadeghian, T. Fujie, X. Shi, S. Cannata, C. Gargioli, A. Tamayol, M.R. Dokmeci, G. Orive, W. Swieszkowski, A. Khademhosseini, 3D Bioprinting in skeletal muscle tissue engineering, Small 15 (2019) 1805530, doi:10.1002/smll.201805530.
[19] J.M. Unagolla, A.C. Jayasuriya, Hydrogel-based 3D bioprinting: a comprehensive review on cell-laden hydrogels, bioink formulations, and future perspectives, Appl. Mater. Today. 18 (2020) 100479, doi:10.1016/j.apmt.2019.100479.
[20] F.L.C. Morgan, L. Moroni, M.B. Baker, Dynamic bioinks to advance bioprinting, Adv. Healthc. Mater. (2020) 1901798, doi:10.1002/adhm.201901798.
[21] R. Levato, T. Jungst, R.G. Scheuring, T. Blunk, J. Groll, J. Malda, From shape to function: the next step in bioprinting, Adv. Mater. 32 (2020) 1906423, doi:10.1002/adma.201906423.
[22] S. Rathan, L. Dejob, R. Schipani, B. Haffner, M.E. Möbius, D.J. Kelly, Fiber reinforced cartilage ECM functionalized bioinks for functional cartilage tissue engineering, Adv. Healthc. Mater. 8 (2019) 1801501, doi:10.1002/adhm.201801501.
[23] A.C. Daly, S.E. Critchley, E.M. Rencsok, D.J. Kelly, A comparison of different bioinks for 3D bioprinting of fibrocartilage and hyaline cartilage, Biofabrication 8 (2016) 045002, doi:10.1088/1758-5090/8/4/045002.
[24] C. Antich, J. de Vicente, G. Jiménez, C. Chocarro, E. Carrillo, E. Montañez, P. Gálvez-Martín, J.A. Marchal, Bio-inspired hydrogel composed of hyaluronic acid and alginate as a potential bioink for 3D bioprinting of articular cartilage engineering constructs, Acta Biomater. 106 (2020) 114–123, doi:10.1016/j.actbio.2020.01.046.
[25] T.J. Levingstone, E. Thompson, A. Matsiko, A. Schepens, J.P. Gleeson, F.J. O'brien, Multi-layered collagen-based scaffolds for osteochondral defect repair in rabbits, Acta Biomater. 32 (2016) 149–160, doi:10.1016/j.actbio.2015.12.034.
[26] H.V. Almeida, R. Eswaramoorthy, G.M. Cunniffe, C.T. Buckley, F.J. O'Brien, D.J. Kelly, Fibrin hydrogels functionalized with cartilage extracellular matrix and incorporating freshly isolated stromal cells as an injectable for cartilage regeneration, Acta Biomater. 36 (2016) 55–62, doi:10.1016/j.actbio.2016.03.008.
[27] S. Hong, D. Sycks, H.F. Chan, S. Lin, G.P. Lopez, F. Guilak, K.W. Leong, X. Zhao, 3D Printing of highly stretchable and tough hydrogels into complex, cellularized structures, Adv. Mater. 27 (2015) 4035–4040, doi:10.1002/adma.201501099.
[28] I.C. Liao, F.T. Moutos, B.T. Estes, X. Zhao, F. Guilak, Composite three-dimensional woven scaffolds with interpenetrating network hydrogels to create functional synthetic articular cartilage, Adv. Funct. Mater. 23 (2013) 5833–5839, doi:10.1002/adfm.201300483.
[29] Y. Sun, Y. You, W. Jiang, Q. Wu, B. Wang, K. Dai, Generating ready-to-implant anisotropic menisci by 3D-bioprinting protein-releasing cell-laden hydrogel-polymer composite scaffold, Appl. Mater. Today 18 (2020) 100469, doi:10.1016/j.apmt.2019.100469.
[30] Y. Dong, X. Sun, Z. Zhang, Y. Liu, L. Zhang, X. Zhang, Y. Huang, Y. Zhao, C. Qi, A.C. Midgley, S. Wang, Q. Yang, Regional and sustained dual-release of growth factors from biomimetic tri-layered scaffolds for the repair of large-scale osteochondral defects, Appl. Mater. Today 19 (2020) 100548, doi:10.1016/j.apmt.2019.100548.
[31] C.W. Peak, K.A. Singh, M. Adlouni, J. Chen, A.K. Gaharwar, Printing therapeutic proteins in 3D using nanoengineered bioink to control and direct cell migration, Adv. Healthc. Mater. 8 (2019) 1801553, doi:10.1002/adhm.201801553.
[32] L.M. Caballero Aguilar, S.M. Silva, S.E. Moulton, Growth factor delivery: defining the next generation platforms for tissue engineering, J. Control. Release. 306 (2019) 40–58, doi:10.1016/j.jconrel.2019.05.028.
[33] T. Gonzalez-Fernandez, S. Rathan, C. Hobbs, P. Pitacco, F.E. Freeman, G.M. Cunniffe, N.J. Dunne, H.O. McCarthy, V. Nicolosi, F.J. O'Brien, D.J. Kelly, Pore-forming bioinks to enable spatio-temporally defined gene delivery in bioprinted tissues, J. Control. Release. 301 (2019) 13–27, doi:10.1016/j.jconrel.2019.03.006.
[34] F.E. Freeman, D.J. Kelly, Tuning alginate bioink stiffness and composition for controlled growth factor delivery and to spatially direct MSC Fate within bioprinted tissues, Sci. Rep. 7 (2017) 1–12, doi:10.1038/s41598-017-17286-1.
[35] R. Chen, Y. Yu, W. Zhang, Y. Pan, J. Wang, Y. Xiao, C. Liu, Tuning the bioactivity of bone morphogenetic protein-2 with surface immobilization strategies, Acta Biomater. 80 (2018) 108–120, doi:10.1016/j.actbio.2018.09.011.
[36] H.V. Almeida, R. Eswaramoorthy, G.M. Cunniffe, C.T. Buckley, F.J. O'Brien, D.J. Kelly, Fibrin hydrogels functionalized with cartilage extracellular matrix and incorporating freshly isolated stromal cells as an injectable for cartilage regeneration, Acta Biomater. 36 (2016) 55–62, doi:10.1016/j.actbio.2016.03.008.
[37] H.V. Almeida, K.J. Mulhall, F.J. O'Brien, D.J. Kelly, Stem cells display a donor dependent response to escalating levels of growth factor release from extracellular matrix-derived scaffolds, J. Tissue Eng. Regen. Med. 11 (2017) 2979–2987, doi:10.1002/term.2199.
[38] Y. Shu, Y. Yu, S. Zhang, J. Wang, Y. Xiao, C. Liu, The immunomodulatory role of sulfated chitosan in BMP-2-mediated bone regeneration, Biomater. Sci. 6 (2018) 2496–2507, doi:10.1039/c8bm00701b.
[39] Q. Feng, S. Lin, K. Zhang, C. Dong, T. Wu, H. Huang, X. Yan, L. Zhang, G. Li, L. Bian, Sulfated hyaluronic acid hydrogels with retarded degradation and enhanced growth factor retention promote hMSC chondrogenesis and articular cartilage integrity with reduced hypertrophy, Acta Biomater. 53 (2017) 329–342, doi:10.1016/j.actbio.2017.02.015.
[40] E. Öztürk, Ø. Arlov, S. Aksel, L. Li, D.M. Ornitz, G. Skjåk-Braek, M. Zenobi-Wong, Sulfated hydrogel matrices direct mitogenicity and maintenance of chondrocyte phenotype through activation of FGF signaling, Adv. Funct. Mater. 26 (2016) 3649–3662, doi:10.1002/adfm.201600092.
[41] I. Freeman, A. Kedem, S. Cohen, The effect of sulfation of alginate hydrogels on the specific binding and controlled release of heparin-binding proteins, Biomaterials 29 (2008) 3260–3268, doi:10.1016/j.biomaterials.2008.04.025.
[42] Y. Yu, R. Chen, Y. Yuan, J. Wang, C. Liu, Affinity-selected polysaccharide for rhBMP-2-induced osteogenesis via BMP receptor activation, Appl. Mater. Today 20 (2020) 100681, doi:10.1016/j.apmt.2020.100681.
[43] S.Y.C. Guo, E.H. Conrad, Process for the sulfation of uronic acid-containing polysaccharides, 2002.
[44] R. Schipani, D.R. Nolan, C. Lally, D.J. Kelly, Integrating finite element modelling and 3D printing to engineer biomimetic polymeric scaffolds for tissue engineering, Connect. Tissue Res. 61 (2020) 174–189, doi:10.1080/03008207.2019.1656720.
[45] Jessica Nulty, Fiona E Freeman, David C Browe, Ross Burdis, Daniel P Ahern, Pierluca Pitacco, Yu Bin Lee, Eben Alsberg, Daniel J Kelly, 3D bioprinting of prevascularised implants for the repair of critically-sized bone defects, Acta Biomater. (2021).
[46] N.Y. Ignat'eva, N.A. Danilov, S.V. Averkiev, M.V. Obrezkova, V.V. Lunin, E.N. Sobol, Determination of hydroxyproline in tissues and the evaluation of the collagen content of the tissues, J. Anal. Chem. 62 (2007) 51–57, doi:10.1134/S106193480701011X.
[47] D.C. Browe, O.R. Mahon, P.J. Díaz-Payno, N. Cassidy, I. Dudurych, A. Dunne, C.T. Buckley, D.J. Kelly, Glyoxal cross-linking of solubilized extracellular matrix to produce highly porous, elastic, and chondro-permissive scaffolds for orthopedic tissue engineering, J. Biomed. Mater. Res. Part A 107 (2019) 2222–2234, doi:10.1002/jbm.a.36731.
[48] L. Fan, L. Jiang, Y. Xu, Y. Zhou, Y. Shen, W. Xie, Z. Long, J. Zhou, Synthesis and anticoagulant activity of sodium alginate sulfates, Carbohydr. Polym. 83 (2011) 1797–1803, doi:10.1016/j.carbpol.2010.10.038.
[49] S. Mohammadi, S. Ramakrishna, S. Laurent, M.A. Shokrgozar, D. Semnani, D. Sadeghi, S. Bonakdar, M. Akbari, Fabrication of nanofibrous PVA/alginate-sulfate substrates for growth factor delivery, J. Biomed. Mater. Res. Part A 107 (2019) 403–413, doi:10.1002/jbm.a.36552.
[50] H. Li, S. Liu, L. Li, Rheological study on 3D printability of alginate hydrogel and effect of graphene oxide, Int. J. Bioprinting 2 (2016) 54–66, doi:10.18063/IJB.2016.02.007.
[51] N. Paxton, W. Smolan, T. Böck, F. Melchels, J. Groll, T. Jungst, Proposal to assess printability of bioinks for extrusion-based bioprinting and evaluation

of rheological properties governing bioprintability, (2017). doi:10.1088/1758-5090/aa8dd8.
[52] Q. Gao, X. Niu, L. Shao, L. Zhou, Z. Lin, A. Sun, J. Fu, Z. Chen, J. Hu, Y. Liu, Y. He, 3D printing of complex GelMA-based scaffolds with nanoclay, Biofabrication 11 (2019) 035006, doi:10.1088/1758-5090/ab0cf6.
[53] W. Liu, M.A. Heinrich, Y. Zhou, A. Akpek, N. Hu, X. Liu, X. Guan, Z. Zhong, X. Jin, A. Khademhosseini, Y.S. Zhang, Extrusion bioprinting of shear-thinning gelatin methacryloyl bioinks, Adv. Healthc. Mater. 6 (2017) 1601451, doi:10.1002/adhm.201601451.
[54] J. Yin, M. Yan, Y. Wang, J. Fu, H. Suo, 3D Bioprinting of low-concentration cell-laden gelatin methacrylate (GelMA) bioinks with a two-step cross-linking strategy, ACS Appl. Mater. Interfaces. 10 (2018) 6849–6857, doi:10.1021/acsami.7b16059.
[55] A.M. McDermott, S. Herberg, D.E. Mason, J.M. Collins, H.B. Pearson, J.H. Dawahare, R. Tang, A.N. Patwa, M.W. Grinstaff, D.J. Kelly, E. Alsberg, J.D. Boerckel, Recapitulating bone development through engineered mesenchymal condensations and mechanical cues for tissue regeneration, Sci. Transl. Med. (2019) 11, doi:10.1126/scitranslmed.aav7756.
[56] J. Visser, F.P.W. Melchels, J.E. Jeon, E.M. Van Bussel, L.S. Kimpton, H.M. Byrne, W.J.A. Dhert, P.D. Dalton, D.W. Hutmacher, J. Malda, Reinforcement of hydrogels using three-dimensionally printed microfibres, Nat. Commun. 6 (2015) 1–10, doi:10.1038/ncomms7933.
[57] K.L. Moffat, K. Goon, F.T. Moutos, B.T. Estes, S.J. Oswald, X. Zhao, F. Guilak, Composite cellularized structures created from an interpenetrating polymer network hydrogel reinforced by a 3D woven scaffold, Macromol. Biosci. 18 (2018) 1800140, doi:10.1002/mabi.201800140.
[58] J. Visser, F.P.W. Melchels, J.E. Jeon, E.M. Van Bussel, L.S. Kimpton, H.M. Byrne, W.J.A. Dhert, P.D. Dalton, D.W. Hutmacher, J. Malda, Reinforcement of hydrogels using three-dimensionally printed microfibres, Nat. Commun. 6 (2015) 1–10, doi:10.1038/ncomms7933.
[59] S. Critchley, E.J. Sheehy, G. Cunniffe, P. Diaz-Payno, S.F. Carroll, O. Jeon, E. Alsberg, P.A.J. Brama, D.J. Kelly, 3D printing of fibre-reinforced cartilaginous templates for the regeneration of osteochondral defects, Acta Biomater. 113 (2020) 130–143, doi:10.1016/j.actbio.2020.05.040.
[60] J. Dinoro, M. Maher, S. Talebian, M. Jafarkhani, M. Mehrali, G. Orive, J. Foroughi, M.S. Lord, A. Dolatshahi-Pirouz, Sulfated polysaccharide-based scaffolds for orthopaedic tissue engineering, Biomaterials 214 (2019) 119214, doi:10.1016/j.biomaterials.2019.05.025.
[61] H.V. Almeida, Y. Liu, G.M. Cunniffe, K.J. Mulhall, A. Matsiko, C.T. Buckley, F.J. O'Brien, D.J. Kelly, Controlled release of transforming growth factor-β3 from cartilage-extra-cellular-matrix-derived scaffolds to promote chondrogenesis of human-joint-tissue-derived stem cells, Acta Biomater. 10 (2014) 4400–4409, doi:10.1016/j.actbio.2014.05.030.
[62] S. Orr, I. Strominger, E. Eremenko, E. Vinogradov, E. Ruvinov, A. Monsonego, S. Cohen, TGF-β affinity-bound to a macroporous alginate scaffold generates local and peripheral immunotolerant responses and improves allocell transplantation, Acta Biomater. 45 (2016) 196–209, doi:10.1016/j.actbio.2016.08.015.
[63] Y. Deng, G. Lei, Z. Lin, Y. Yang, H. Lin, R.S. Tuan, Engineering hyaline cartilage from mesenchymal stem cells with low hypertrophy potential via modulation of culture conditions and Wnt/β-catenin pathway, Biomaterials 192 (2019) 569–578, doi:10.1016/j.biomaterials.2018.11.036.
[64] P. Yeung, W. Zhang, X.N. Wang, C.H. Yan, B.P. Chan, A human osteoarthritis osteochondral organ culture model for cartilage tissue engineering, Biomaterials 162 (2018) 1–21, doi:10.1016/j.biomaterials.2018.02.002.
[65] K. Liu, G.D. Zhou, W. Liu, W.J. Zhang, L. Cui, X. Liu, T.Y. Liu, Y. Cao, The dependence of in vivo stable ectopic chondrogenesis by human mesenchymal stem cells on chondrogenic differentiation in vitro, Biomaterials 29 (2008) 2183–2192, doi:10.1016/j.biomaterials.2008.01.021.
[66] M.N. George, X. Liu, A.L. Miller, H. Xu, L. Lu, Phosphate functionalization and enzymatic calcium mineralization synergistically enhance oligo [poly(ethylene glycol) fumarate] hydrogel osteoconductivity for bone tissue engineering, J. Biomed. Mater. Res. Part A. 108 (2020) 515–527, doi:10.1002/jbm.a.36832.